

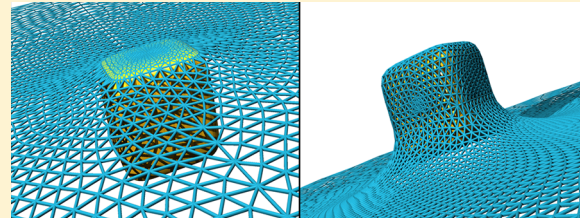
# Shape and Orientation Matter for the Cellular Uptake of Nonspherical Particles

Sabyasachi Dasgupta, Thorsten Auth, and Gerhard Gompper\*

Theoretical Soft Matter and Biophysics, Institute of Complex Systems and Institute for Advanced Simulation, Forschungszentrum Jülich, D-52425 Jülich, Germany

## Supporting Information

**ABSTRACT:** Recent advances in nanotechnology have made a whole zoo of particles of different shapes available for applications, but their interaction with biological cells and their toxicity is often not well understood. Experiments have shown that particle uptake by cells is determined by an intricate interplay between physicochemical particle properties like shape, size, and surface functionalization, but also by membrane properties and particle orientation. Our work provides systematic understanding, based on a mechanical description, for membrane wrapping of nanoparticles, viruses, and bacterial forms. For rod-like particles, we find stable endocytotic states with small and high wrapping fraction; an increased aspect ratio is unfavorable for complete wrapping. For high aspect ratios and round tips, the particles enter via a submarine mode, side-first with their long edge parallel to the membrane. For small aspect ratios and flat tips, the particles enter tip-first via a rocket mode.



**KEYWORDS:** Nanoparticle uptake, passive endocytosis, nanoparticle shape, nanoparticle size, continuum membrane model, wrapping energy

Transport within a biological cell and exchange of material across its membrane are basic processes that the cell uses to interact with its environment. Depending on size, shape, and surface properties, nanoparticles and micro-organisms can cross a cellular membrane either by penetration<sup>1–3</sup> or wrapping. For example, filoviruses<sup>4,5</sup> and also brick-shaped intracellular mature virions<sup>6</sup> of the family Poxviridae (fowl-pox and pigeon-pox) get wrapped by the host plasma membrane. In particular, the Ebola<sup>4,5</sup> and the Marburg virus<sup>5</sup> are of much interest due to their enhanced virulence leading to high mortality rates. Their prolonged blood circulation time has inspired development of tubular filamentous vehicles<sup>7</sup> as potential drug-delivery agents for treating cancer. While wrapping of spherical particles has been studied in great detail,<sup>8–11</sup> there is no systematic study and understanding for the wrapping of nonspherical particles.<sup>12–17</sup>

Elongated viruses,<sup>4–6</sup> such as Ebola, Marburg, and pox viruses, as well as the bullet-shaped Rhabdoviruses,<sup>18,19</sup> exhibit competition between a submarine and a rocket mode for cell entry via membrane wrapping. In submarine mode, the long axis of the virus is oriented parallel to the membrane and in rocket mode, it is oriented perpendicular to the membrane. Similar modes for uptake have been reported for rod-like nanoparticles<sup>15–17,20</sup> and multiwall carbon nanotubes.<sup>21</sup> The aspect ratio is an important parameter to characterize the shape of elongated particles. Experimentally, a high aspect ratio has been found to suppress uptake compared to spherical particles of a similar size.<sup>15,16</sup> More recently, uptake experiments with cube-like particles have been performed,<sup>17,22</sup> but there is no

systematic study for different sizes available so far. However, experiments and molecular dynamics simulations that show a role of shape,<sup>23–26</sup> aspect ratio,<sup>15–17,20</sup> and orientation<sup>1,27–30</sup> stress the importance of these geometric parameters for cellular uptake and toxicity studies.

Physically, nanoparticle attachment and wrapping are controlled by the competition between the adhesion-energy gain for contact between a nanoparticle and a membrane and the deformation-energy cost for the lipid bilayer. Attachment (binding) occurs when the adhesion strength is large enough to compensate the local bending-energy cost at the surface point of smallest curvature. This binding transition is predicted to be continuous<sup>11,31</sup> (without an energy barrier). For higher values of the adhesion strength between particle and membrane, a discontinuous transition (with an energy barrier) occurs either between two frustrated endocytotic, partially wrapped states or between a partially wrapped and the completely wrapped state. Only in the case of spherical particles and for a vanishing membrane tension the entire wrapping process is continuous. Special cases of wrapping of nonspherical nanoparticles have been addressed theoretically, such as the enhanced stability of partially wrapped states for soft<sup>32</sup> and ellipsoidal<sup>31</sup> nanoparticles, the reorientation of ellipsoidal<sup>33</sup> and spherocylindrical<sup>27,34</sup> nanoparticles during uptake, and the perpendicular

**Received:** October 22, 2013

**Revised:** December 21, 2013

**Published:** January 2, 2014

entry of cylindrical nanoparticles.<sup>27</sup> Many of these studies have been performed by molecular dynamics simulations.

In our work, we systematically investigate the role of nanoparticle shape (Figure 1) and size, as well as membrane

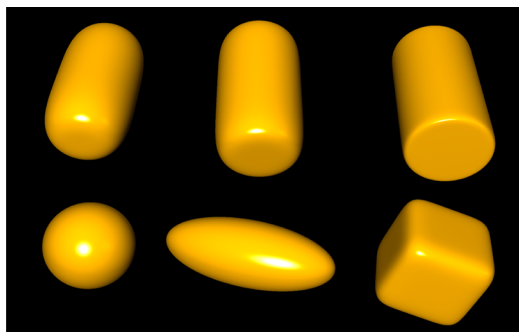


**Figure 1.** Shapes of nonspherical nanoparticles. Top row: rod-like particles of aspect ratio  $b/a = 2$  with blunt tips and increasing edge curvature, defined by  $[(x^2 + y^2)/a^2]^{(n/2)} + (z/b)^n = 1$  with  $n = 4$ ,  $n = 6$ , and  $n = 20$ . Bottom row: sphere, ellipsoid, Hauser's cube. We characterize the particles by their size  $a$ , which is the radius of the sphere, the half edge-length of the cube, and the short axis of the ellipsoidal and rod-like particles.

bending rigidity and tension, on membrane wrapping and cellular uptake. We predict phase diagrams for two classes of nanoparticles, nanorods, and nanocubes, with varying the aspect ratio and edge curvature. Possible modes of entry for elongated particles are shown in Figure 2. Our phase diagrams for nanorods show a qualitatively different wrapping behavior compared to nanospheres and nanoellipsoids. In particular, we find two distinct partial-wrapped states, with shallow and deep wrapping. We show that global parameters like particle size and aspect ratio alone are by far not sufficient to determine particle endocytosis. Instead, local geometrical properties, such as the extrema of the local mean curvature, matter and change the wrapping behavior qualitatively.

All of our calculations are based on the curvature energy<sup>35</sup> of lipid-bilayer membranes combined with a contact adhesion

energy for the particle–membrane interaction. Thus, the total energy is

$$\epsilon_{\text{tot}} = \int_S dS [2\kappa H^2 + \sigma] - w \int_{S_{\text{ad}}} dS \quad (1)$$

where  $S$  is the entire membrane area,  $S_{\text{ad}}$  the adhered membrane area,  $H$  the mean membrane curvature,  $\kappa$  the bending rigidity,  $\sigma$  the membrane tension, and  $w$  the adhesion strength for the interaction between membrane and nanoparticle. We use triangulated membranes and the Surface Evolver to minimize the membrane deformation energies.<sup>36,37</sup>

We model cube-like particles as Hauser's cube using  $x^6 + y^6 + z^6 = a^6$  and rod-like particles using  $[(x^2 + y^2)/a^2]^{(n/2)} + (z/b)^n = 1$  as regular ellipsoids with  $n = 2$  and as supereggs with  $n \geq 4$ . We consider nanorods with aspect ratios  $1 \leq b/a \leq 3$  and  $n = 4$  as well as  $n = 6$ ; high values of  $n$  correspond to very flat tips, such that the shape becomes cylinder-like. We describe our system using a characteristic length scale, such as the particle size  $a$  (Figure 1), typically 20–100 nm and a characteristic energy scale, such as the bilayer bending rigidity  $\kappa$ , typically  $10 - 100 k_B T$ . We then define dimensionless parameters, like the reduced deformation energy  $\tilde{\epsilon} = \epsilon_{\text{tot}}/\pi\kappa$ , the reduced membrane tension  $\tilde{\sigma} = \sigma a^2/\kappa$ , and the reduced adhesion strength  $\tilde{w} = wA/2\pi\kappa$ , where  $A$  is the particle surface area. Using these parameters for the axes of our phase diagrams, our predictions apply for arbitrary particle sizes.

We first consider the uptake of ellipsoidal nanoparticles. Recent experimental<sup>14,38</sup> and theoretical<sup>31</sup> work shows enhanced binding, but lower uptake compared with spherical particles. For these particles, an extended region of the phase diagram exists with stable, frustrated endocytotic states at low wrapping fractions for which the long axis is oriented parallel to the membrane (Figure 2c). A reorientation from parallel to perpendicular upon increased wrapping has been suggested recently.<sup>33</sup> We have determined phase diagrams for this system (see the Supporting Information) and confirm the presence of a perpendicular state at a high wrapping fraction. In addition, we predict the complete-wrapping transition to be continuous. Surprisingly, our results show that, after reorientation from

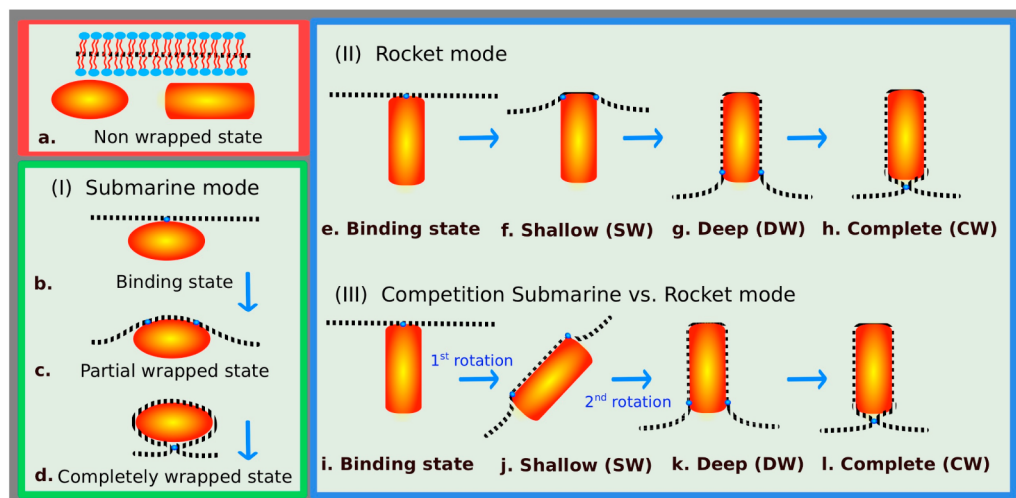


**Figure 2.** Modes of entry for nanoparticle uptake by membrane wrapping: (I) submarine mode with the long axis of the particles oriented parallel to the membrane, (II) rocket mode with the long axis oriented perpendicular to the membrane, and (III) competition between submarine and rocket mode as observed for rod-like particles with high aspect ratios. The complete-wrapped particle is connected by an infinitely small catenoidal neck to the membrane; the particle orientation in this state is irrelevant.

parallel to perpendicular, the adhesion strength required for complete wrapping is well above the adhesion strength required without reorientation. Reorientation thus leads to unfavorable, arrested endocytotic states (analogously to Figure 2g), because wrapping the highly curved tip of the ellipsoid requires a high bending energy cost per area. Thus, a suppression of reorientation, as it might occur for fast wrapping, facilitates particle uptake.

The wrapping of cube-like and rod-like particles compared to the wrapping of spheres and ellipsoids is qualitatively different. For nanocubes, the binding occurs for almost vanishing adhesion strength with a “flat” side oriented toward the membrane (Figure 3a), because it requires hardly any membrane deformation. The bound state corresponds to the shallow-wrapped state (SW) that is separated by an energy barrier from the deep-wrapped state (DW) in Figure 3b. The transition from the deep-wrapped to the complete-wrapped state (CW) is also discontinuous, which further stabilizes the partially wrapped states. The existence of shallow- and deep-wrapped states is a consequence of the inhomogeneous curvature distribution on the nanoparticle surface. The adhesion strength has to exceed a threshold for the adhesion energy of the lateral sides of the cube to compensate the deformation energy at the upper edges of the cube in Figure 3a. The deformation energy at the lower edges is even higher, because the membrane now has to nearly double back on itself, so that complete wrapping requires an even larger  $w$ . Note that a discontinuous transition between the DW and CW states does not exist for ellipsoids, because the curvature maxima are point-like (see Supporting Information). The dependence of the phase boundaries on particle size  $a$  is taken into account by our dimensionless variables. The values of adhesion strength  $w$  and membrane tension  $\sigma$  for the phase transitions scale directly with the squared particle size  $a$  and inversely with the membrane bending modulus  $\kappa$ .

Figure 3c shows the phase diagram for wrapping of a nanocube. Because of the flat sides, the shallow-wrapped region starts for infinitesimal adhesion strength  $w$ . However, the translational and orientational entropy of the cube in the unbound state competes with the energy gain for adhesion. Adhesion therefore occurs only if  $wa^2 \gtrsim k_B T$ . In terms of the phase diagram, the unbound region due to entropy is a very small stripe for small adhesion strength of width  $k_B T/\kappa$  (not shown). Deep wrapping occurs for an adhesion strength that is about twice the adhesion strength for complete wrapping of a sphere with an equal surface area,  $w_{\text{sph}} = 2\kappa/a^2$ . Complete wrapping is found for an adhesion strength about three times higher than for a sphere. With increased membrane tension, both transitions from the shallow- to the deep-wrapped state ( $W_2$ ) and from the deep-wrapped to the complete-wrapped state ( $W_3$ ) shift to higher adhesion strengths.

Next, we consider rod-like particles with blunt tips and different edge curvatures, characterized by the parameter  $n$  and the aspect ratio; see Figure 1. Phase diagrams are shown in Figure 4. At negligible membrane tension, the transition  $W_2$  between shallow-wrapped and deep-wrapped states corresponds to adhesion strengths that are comparable with those required for complete wrapping of spherical particles; the transition shifts to higher adhesion strengths with increasing membrane tension. The envelopment transition  $W_3$  is largely independent of the membrane tension, because the change in wrapped area between deep-wrapped and complete-wrapped state is small. Both increased aspect ratio and sharper edges

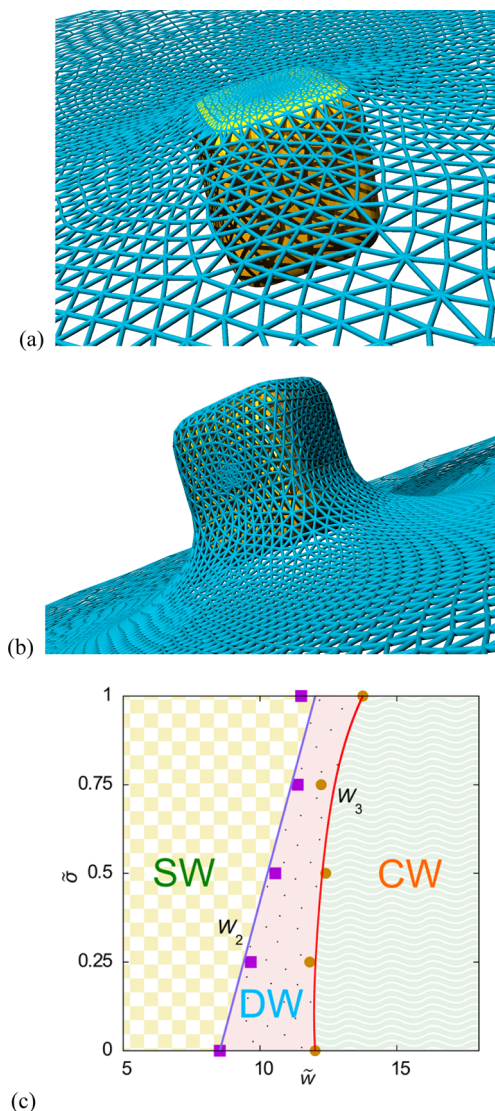


**Figure 3.** (a, b) Membrane deformation for wrapping of Hauser’s cube. The network of edges and triangles describes the membrane shape and is used for the numerical calculation of the curvature energy. Membrane conformations are shown at fixed tension  $\tilde{\sigma} = 0.50$  for two corresponding states at the  $W_2$  phase boundary: (a) a shallow-wrapped state with approximately 10% of particle wrapped, and (b) a deep-wrapped state with a wrapping fraction of approximately 80%. (c) Phase diagram for wrapping of Hauser’s cube for membrane tension  $\tilde{\sigma}$  and adhesion strength  $\tilde{w}$ ; the parameters are given in dimensionless form. We find a shallow-wrapped (SW), a deep-wrapped (DW), and a complete-wrapped (CW) state, separated by two discontinuous wrapping transitions,  $W_2$  and  $W_3$ .

suppress uptake, as can be seen in the phase diagrams of Figure 4 by the shift of the  $W_3$  transition to higher adhesion strengths,  $\tilde{w}$ . The parameter region for the deep-wrapped state widens with increasing aspect ratio, because the transition from the shallow-wrapped to the deep-wrapped state remains almost unaltered. This is due to the competition between the larger adhesion energy gain at the sides of the particles for higher aspect ratios and the increasing edge curvature (for fixed particle area).

Rod-like particles first bind with the long axis perpendicularly to the membrane<sup>30</sup> (Figure 2e), because adhesion at the blunt tips minimizes the deformation energy cost. For rounded edges

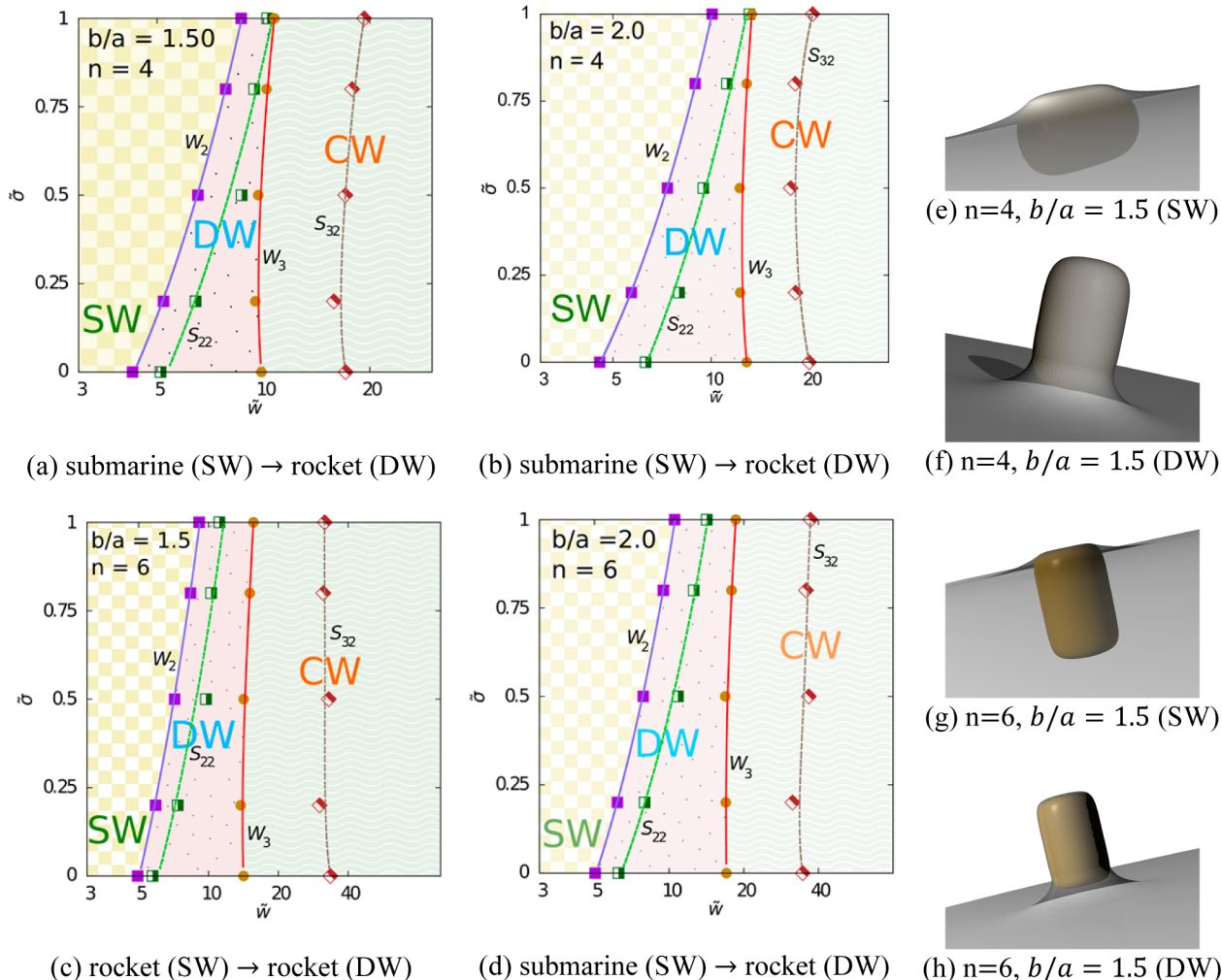


**Figure 4.** (a–d) Phase diagrams for wrapping of rod-like particles with equal surface areas and various aspect ratios, showing shallow-wrapped (SW), deep-wrapped (DW), and complete-wrapped (CW) states. A discussion for the cases of equal size  $a$  and equal volume (for a spherocylinder) is presented in the Supporting Information. (e–h) Membrane and particle conformations for submarine and rocket states. As indicated below the phase diagrams, in most cases the transition from the SW to the DW state is associated with a reorientation of the particle from submarine to rocket orientation. For the special case of aspect ratio 1.5 and  $n = 6$ , the particle is in rocket orientation in both the shallow-wrapped and the deep-wrapped state.

( $n = 4$ ) or higher aspect ratios (Figure 4a, b, and d), the particle switches to parallel orientation (Figure 4e) after initial binding and back to perpendicular orientation for the deep-wrapped state (Figure 4f). However, for the special case of sharper edges ( $n = 6$ ) and aspect ratio 1.5 (Figure 4c), the particle enters in rocket mode only (Figure 4g and h). In virus and nanotube uptake experiments,<sup>4–6</sup> both submarine and rocket modes have indeed been observed.

We have characterized the critical wrapping fractions for both stable states in Figure 5a and b. For the transition between shallow-wrapped and deep-wrapped states ( $W_2$ ), and for both aspect ratios 1.5 and 2, the wrapping fraction jumps from about 10% to about 80%. For the envelopment transition ( $W_3$ ), the wrapping fraction jumps from 80–90% to complete wrapping. For both discontinuous transitions,  $W_2$  and  $W_3$ , we have also estimated spinodals ( $S_{22}$  and  $S_{32}$  in Figure 4) for spontaneous wrapping and upper bounds for the energy barriers (Figure 5c and d). The energy barriers,  $\Delta E_{\text{bar}}(W_2)$  and  $\Delta E_{\text{bar}}(W_3)$ , are of the order of  $\pi\kappa$ . Both the energy barriers and the associated spinodals for the  $W_2$  transitions (shallow- to deep-wrapped) are approximate values, because of the piecewise nature of the

energy profile in our calculations (see Supporting Information). By calculating the wrapping energies for all possible orientations, exact values for energy barriers and spinodals can be obtained, but the phase boundaries remain unaffected. The energy barriers and spinodals for the  $W_3$  transition (deep- to complete-wrapped) are not connected with any orientation changes and are therefore exact; spontaneous complete wrapping occurs for adhesion strengths that are as much as 5–10 times higher than for spherical nanoparticles.

To elucidate the role of particle shape further, we show in Figures 6 and 7 wrapping phase diagrams of nanorods as function of edge curvature and particle aspect ratio, respectively, both for fixed particle surface areas. Figure 6 displays the wrapping states for varying edge sharpness in case of a tensionless membrane, at fixed aspect ratios  $b/a = 1$  and  $b/a = 2$ . For spherical particles (Figure 6a,  $n = 2$ ), the nonwrapped state directly transits to the completely wrapped state, whereas for ellipsoidal particles (Figure 6b,  $n = 2$ ), a partially wrapped state can exist even for a tensionless membrane due to the high curvature at the tips. The sharp edges of rod-like particles with  $n > 2$  imply two discontinuous

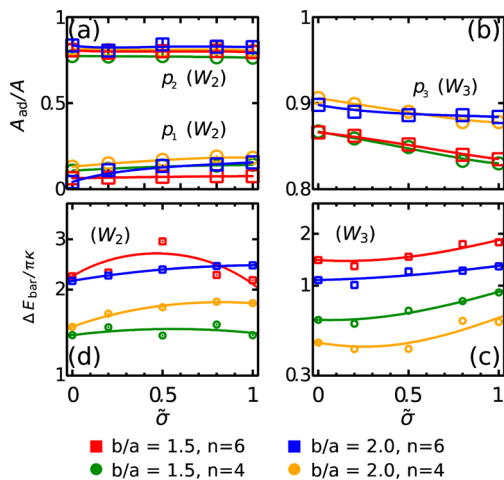


**Figure 5.** (a, b) Wrapping fractions for stable states for the discontinuous wrapping transitions  $W_2$  and  $W_3$  for aspect ratios 1.5 and 2 and for  $n = 4$  and 6. The shallow-wrapped states correspond to wrapping fractions of 10–20%, the deep-wrapped states to wrapping fractions of 80–90%. (c, d) The energy barriers for both transitions, between the shallow-wrapped and the deep-wrapped state and between the deep-wrapped and the complete-wrapped state, are of the order  $\pi\kappa$  and increase with the sharpness of the edges.

transitions,  $W_2$  and  $W_3$ , separating shallow-wrapped and deep-wrapped, and deep-wrapped and complete-wrapped states. The deep-wrapped regime extends strongly with increasing edge sharpness. Because of locally flat parts of their surface, rod-like nanoparticles adhere to the membrane already for very small adhesion strengths, in contrast to spheres and ellipsoids. For rod-like nanoparticles with  $b/a = 1$ , the rocket orientation is preferred for both partially wrapped states independent of edge sharpness; for  $b/a = 2$ , nanoparticles reorient from submarine to rocket orientation when they cross the discontinuous transition  $W_2$ .

Figure 7 shows the wrapping states for rod-like nanoparticles with smoother ( $n = 4$ ) and sharper edges ( $n = 6$ ) as a function of the aspect ratio, with  $1 \leq b/a \leq 3$ . Increased edge sharpness increases the regime with rocket orientation in the shallow-wrapped state but hardly affects the phase boundary between shallow-wrapped and deep-wrapped states. However, the phase boundary between deep-wrapped and complete-wrapped states shifts significantly to larger adhesion strengths for increased edge sharpness.

Interaction with cells and a successful passage through the plasma membrane is the primary step both for applications and the toxicity of nanoparticles. The versatile properties of nanoparticles predicted by our model of nonspherical nanoparticles provide interesting perspectives for their use as biosensors for optical imaging,<sup>39,40</sup> as membrane–protein binding sensors,<sup>40</sup> as drug delivery agents, and for use in photochemical treatment<sup>22</sup> using surface plasmon resonance techniques. Also, wrapping in systems containing many spherical colloidal particles can be rationalized by our model of elongated particles. Partially attached spherical particles aggregate<sup>41,42</sup> and form necklace-like linear and tubular aggregates on the membrane<sup>43,44</sup> with increased adhesion strength. This is analogous to our frustrated endocytotic states with parallel and perpendicular orientation of rod-like colloids to the membrane. In Table 1, we summarize basic properties for wrapping of particles with different shapes as necessary prerequisites for predicting any desired or toxic effects.

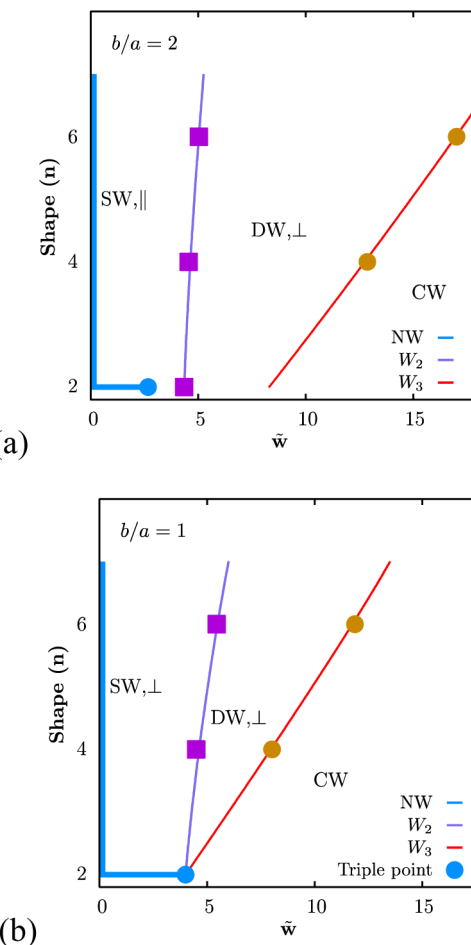


**Figure 6.** Role of edge curvature (characterized by  $n$ ) on the wrapping behavior of a tensionless membrane for nanoparticles with fixed aspect ratio (a)  $b/a = 1$  and (b)  $b/a = 2$ . The particle orientation in the shallow-wrapped (SW) and deep-wrapped (DW) states is indicated by the symbols  $\perp$  and  $\parallel$ , corresponding to rocket and submarine orientation, respectively. Nonwrapped states are marked by light-blue lines.

Our results emphasize the importance for both calculations using continuum membranes in equilibrium that provide a systematic understanding of wrapping energies<sup>11,31,43–45</sup> and dynamic molecular simulations<sup>1,27,28,34</sup> that add details for specific systems and further investigate dynamical aspects of the budding pathway.

Based on energy minimization, we find two different modes with parallel and perpendicular orientation for entry of elongated particles into cells. Particles with a high aspect ratio bind in parallel orientation but transit from deep to complete wrapping in perpendicular orientation. However, a major part of the wrapping process for spherocylinders studied in ref 27 seems to occur in parallel orientation. Parallel orientation favors complete wrapping, because a stable deep-wrapped state is avoided (see the Supporting Information). Calculations for specific particle sizes, which include dynamical, nonequilibrium aspects, show that the orientation also depends on the speed of internalization;<sup>21,34</sup> such dynamical calculations thus complement our systematic study of the influence of particle shape in equilibrium.

Our basic wrapping picture can be modified by additional parameters, such as surface functionalization or the more complex structure of the cell membrane. Surface functionaliza-

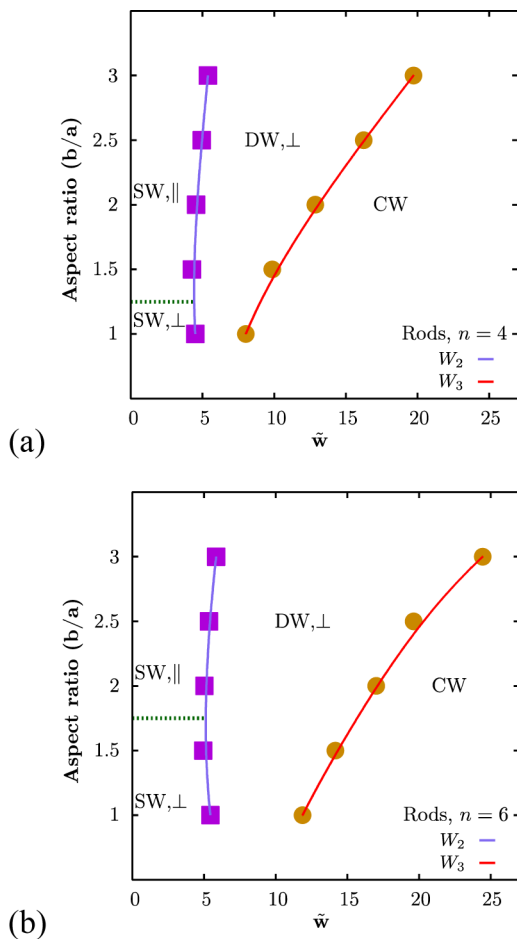


**Figure 7.** Role of aspect ratio on the wrapping behavior of a tensionless membrane for rod-like nanoparticles with (a) smoother edges ( $n = 4$ ) and (b) sharper edges ( $n = 6$ ). The particle orientation in the shallow-wrapped (SW) to deep-wrapped states (DW) is indicated by the symbols  $\perp$  and  $\parallel$ , corresponding to rocket and submarine orientation, respectively.

tion<sup>20,46</sup> or coating of nanoparticles by corona proteins is captured by our model, as long as the particle's surface properties are homogeneous and can be expressed by an overall adhesion strength  $w$ . Inhomogeneous surface coatings require more detailed models and calculations. Also, a multicomponent

membrane or the cell cytoskeleton may have to be taken into account for specific wrapping calculations, such as phagocytosis of *E. coli* with a high aspect ratio. In this case, the cytoskeleton plays a significant role, and contrary to our predictions, high aspect-ratio bacteria with rounded ends are wrapped starting at the tip in a "race to the pole".<sup>30</sup> However, this does not invalidate our calculations based on membrane mechanics but rather indicates that further energy or dynamic contributions may have to be taken into account.

## ■ ASSOCIATED CONTENT

### Supporting Information

Details about numerical calculations. Additional information on geometrical properties of the investigated nanoparticles. Wrapping energies as a function of the wrapping fraction. Further phase diagrams for spheres, ellipsoids, rod-like particles, spherocylinders, and nanocubes. This material is available free of charge via the Internet at <http://pubs.acs.org>.

## ■ AUTHOR INFORMATION

### Corresponding Author

\*E-mail: g.gompper@fz-juelich.de.

### Notes

The authors declare no competing financial interest.

## ■ ACKNOWLEDGMENTS

We thank K. Brakke (Selinsgrove, PA) for his advice on Surface Evolver and for helpful discussions on numerical techniques and R. Korenstein (Tel Aviv) for stimulating discussions on nanoparticles at membranes. Support from the EU FP7 NMP collaborative project PreNanoTox (309666) is gratefully acknowledged. S.D. acknowledges support from the International Helmholtz Research School of Biophysics and Soft Matter (IHRs BioSoft).

## ■ REFERENCES

- (1) Yang, K.; Ma, Y.-Q. *Nat. Nanotechnol.* **2010**, *5*, 579–583.
- (2) Pogodin, S.; Werner, M.; Sommer, J.-U.; Baulin, V. A. *ACS Nano* **2012**, *6*, 10555–10561.
- (3) Pogodin, S.; Baulin, V. A. *ACS Nano* **2010**, *4*, 5293–5300.
- (4) Noda, T.; Ebihara, H.; Muramoto, Y.; Fujii, K.; Takada, A.; Sagara, H.; Kim, J. H.; Kida, H.; Feldmann, H.; Kawaoka, Y. *PLoS Pathog.* **2006**, *2*, e99.
- (5) Welsch, S.; Kolesnikova, L.; Krähling, V.; Riches, J. D.; Becker, S.; Briggs, J. A. *PLoS Pathog.* **2010**, *6*, e1000875.

**Table 1. Shape Dependence of Particle Wrapping, Based on References 11 and 31 and This Work<sup>a</sup>**

particle shape	membrane	binding transition	shallow-wrapped state	deep-wrapping transition	deep-wrapped state	envelopment transition
spherical	$\kappa$	cont., for $w = 2\kappa/a^2$				$\equiv$ binding
spherical	$\kappa$ and $\sigma$	cont., for $w = 2\kappa/a^2$	yes			discont.
ellipsoidal	$\kappa$ , $\kappa$ , and $\sigma$	cont., indep. of $\sigma$	yes, submarine	discont., reorient.	yes, rocket	cont.
ellipsoidal (*)	$\kappa$ , $\kappa$ , and $\sigma$	cont., indep. of $\sigma$	yes, submarine			discont.
cube-like	$\kappa$ , $\kappa$ , and $\sigma$	at vanishing $w$	yes	discont.	yes	discont.
spherocylinder	$\kappa$ , $\kappa$ , and $\sigma$	at vanishing $w$ , rocket	yes, submarine	discont., reorient.	yes, rocket	discont.
rod-like	$\kappa$ , $\kappa$ , and $\sigma$	at vanishing $w$ , rocket	yes, submarine	discont., reorient.	yes, rocket	discont.
rod-like (*)	$\kappa$ , $\kappa$ , and $\sigma$	at vanishing $w$ , rocket	yes, submarine			discont.
rod-like (**)	$\kappa$ , $\kappa$ , and $\sigma$	at vanishing $w$ , rocket	yes, rocket	discont.	yes, rocket	discont.

<sup>a</sup>The membrane can be characterized by bending rigidity only, " $\kappa$ ", or by bending rigidity and membrane tension, " $\kappa$  and  $\sigma$ "; the binding transition can occur at finite or vanishing adhesion strength  $w$ ; the particle can be in submarine or rocket orientation; transitions can be continuous (cont.) or discontinuous (discont.) and may involve reorientation (reorient.). The binding transition for ellipsoids is independent of the membrane tension and is given in ref 31. (\*) Fast wrapping at high adhesion strength, such that a bound ellipsoid cannot reorient to rocket orientation. (\*\*) Rocket mode for supereggs with blunt tips and small aspect ratio (e.g.,  $n = 4$  and  $b/a = 1.5$ ).

- (6) Hatano, Y.; Yoshida, M.; Uno, F.; Yoshida, S.; Osafune, N.; Ono, K.; Yamada, M. *J. Electron Microsc.* **2001**, *50*, 113–124.
- (7) Geng, Y.; Dahaimer, P.; Cai, S.; Tsai, R.; Tewari, M.; Minko, T.; Discher, D. E. *Nat. Nanotechnol.* **2007**, *2*, 249–255.
- (8) Zhang, S.; Li, J.; Lykotrafitis, G.; Bao, G.; Suresh, S. *Adv. Mater.* **2009**, *21*, 419–424.
- (9) Zhang, S.; Nelson, A.; Beales, P. A. *Langmuir* **2012**, *28*, 12831–12837.
- (10) Gao, H.; Shi, W.; Freund, L. B. *Proc. Natl. Acad. Sci. U.S.A.* **2005**, *102*, 9469–9474.
- (11) Deserno, M. *Phys. Rev. E* **2004**, *69*, 031903.
- (12) Jiang, W.; Kim, B. Y.; Rutka, J. T.; Chan, W. C. *Nat. Nanotechnol.* **2008**, *3*, 145–150.
- (13) Adriani, G.; de Tullio, M. D.; Ferrari, M.; Hussain, F.; Pascazio, G.; Liu, X.; Decuzzi, P. *Biomaterials* **2012**, *33*, 5504–5513.
- (14) Zhang, Y.; Tekobo, S.; Tu, Y.; Zhou, Q.; Jin, X.; Dergunov, S. A.; Pinkhassik, E.; Yan, B. *ACS Appl. Mater. Interfaces* **2012**, *4*, 4099–4105.
- (15) Chithrani, B. D.; Ghazani, A. A.; Chan, W. C. *Nano Lett.* **2006**, *6*, 662–668.
- (16) Chithrani, B. D.; Chan, W. C. *Nano Lett.* **2007**, *7*, 1542–1550.
- (17) Gratton, S. E.; Ropp, P. A.; Pohlhaus, P. D.; Luft, J. C.; Madden, V. J.; Napier, M. E.; DeSimone, J. M. *Proc. Natl. Acad. Sci. U.S.A.* **2008**, *105*, 11613–11618.
- (18) Cureton, D. K.; Massol, R. H.; Saffarian, S.; Kirchhausen, T. L.; Whelan, S. P. *PLoS Pathog.* **2009**, *5*, e1000394.
- (19) Ge, P.; Tsao, J.; Schein, S.; Green, T. J.; Luo, M.; Zhou, Z. H. *Science* **2010**, *327*, 689–693.
- (20) Qiu, Y.; Liu, Y.; Wang, L.; Xu, L.; Bai, R.; Ji, Y.; Wu, X.; Zhao, Y.; Li, Y.; Chen, C. *Biomaterials* **2010**, *31*, 7606–7619.
- (21) Shi, X.; von dem Bussche, A.; Hurt, R. H.; Kane, A. B.; Gao, H. *Nat. Nanotechnol.* **2011**, *6*, 714–719.
- (22) Wang, Y.; Black, K. C.; Luehmann, H.; Li, W.; Zhang, Y.; Cai, X.; Wan, D.; Liu, S.-Y.; Li, M.; Kim, P. *ACS Nano* **2013**, *7*, 2068–2077.
- (23) Best, J. P.; Yan, Y.; Caruso, F. *Adv. Healthcare Mater.* **2012**, *1*, 35–47.
- (24) Decuzzi, P.; Pasqualini, R.; Arap, W.; Ferrari, M. *Pharm. Res.* **2009**, *26*, 235–243.
- (25) Champion, J. A.; Mitragotri, S. *Proc. Natl. Acad. Sci. U.S.A.* **2006**, *103*, 4930–4934.
- (26) Mitragotri, S.; Lahann, J. *Nat. Mater.* **2009**, *8*, 15–23.
- (27) Vácha, R.; Martinez-Veracoechea, F. J.; Frenkel, D. *Nano Lett.* **2011**, *11*, 5391–5395.
- (28) Yang, K.; Yuan, B.; Ma, Y.-q. *Nanoscale* **2013**, *5*, 7998–8006.
- (29) Herd, H.; Daum, N.; Jones, A. T.; Huwer, H.; Ghandehari, H.; Lehr, C.-M. *ACS Nano* **2013**, *7*, 1961–1973.
- (30) Möller, J.; Luehmann, T.; Hall, H.; Vogel, V. *Nano Lett.* **2012**, *12*, 2901–2905.
- (31) Dasgupta, S.; Auth, T.; Gompper, G. *Soft Matter* **2013**, *9*, 5473–5482.
- (32) Yi, X.; Shi, X.; Gao, H. *Phys. Rev. Lett.* **2011**, *107*, 098101.
- (33) Bahrami, A. H. *Soft Matter* **2013**, *9*, 8642–8646.
- (34) Huang, C.; Zhang, Y.; Yuan, H.; Gao, H.; Zhang, S. *Nano Lett.* **2013**, *13*, 4546–4550.
- (35) Helfrich, W. Z. *Naturforsch. C* **1973**, *28*, 693.
- (36) Gompper, G.; Kroll, D. M. Triangulated-Surface Models of Fluctuating Membranes. In *Statistical Mechanics of Membranes and Surfaces*, 2nd ed.; Nelson, D. R., Piran, T., Weinberg, S., Eds.; World Scientific: Singapore, 2004; pp 359–426.
- (37) Brakke, K. A. *Exp. Math.* **1992**, *1*, 141–165.
- (38) Florez, L.; Herrmann, C.; Cramer, J. M.; Hauser, C. P.; Koynov, K.; Landfester, K.; Crespy, D.; Mailänder, V. *Small* **2012**, *8*, 2222–2230.
- (39) Wang, Y.; Liu, Y.; Luehmann, H.; Xia, X.; Wan, D.; Cutler, C.; Xia, Y. *Nano Lett.* **2013**, *13*, 581–585.
- (40) Wu, H.-J.; Henzie, J.; Lin, W.-C.; Rhodes, C.; Li, Z.; Sartorel, E.; Thorner, J.; Yang, P.; Groves, J. T. *Nat. Methods* **2012**, *9*, 1189–1191.
- (41) Reynwar, B. J.; Illya, G.; Harmandaris, V. A.; Müller, M. M.; Kremer, K.; Deserno, M. *Nature* **2007**, *447*, 461–464.
- (42) Auth, T.; Gompper, G. *Phys. Rev. E* **2009**, *80*, 031901.
- (43) Šarić, A.; Cacciuto, A. *Phys. Rev. Lett.* **2012**, *109*, 188101.
- (44) Bahrami, A. H.; Lipowsky, R.; Weikl, T. R. *Phys. Rev. Lett.* **2012**, *109*, 188102.
- (45) Weikl, T. R. *Eur. Phys. J. E* **2003**, *12*, 265–273.
- (46) Barua, S.; Yoo, J.-W.; Kolhar, P.; Wakankar, A.; Gokarn, Y. R.; Mitragotri, S. *Proc. Natl. Acad. Sci. U.S.A.* **2013**, *110*, 3270–3275.